Volume 3 | Number 9 | September 2016

INORGANIC CHEMISTRY

FRONTIERS

Chinese Chemical Society

ROYAL SOCIETY OF CHEMISTRY

http://rsc.li/frontiers-inorganic

INORGANIC CHEMISTRY
FRONTIERS

RESEARCH ARTICLE

Cite this: *Inorg. Chem. Front.*, 2016, **3**, 1137

Promoted hydrogen release from alkali metal borohydrides in ionic liquids†

He Fu,[a] Yong Wu,[a] Jun Chen,[a] Xiaojuan Wang,[b] Jie Zheng*[a] and Xingguo Li*[a]

Received 1st June 2016,
Accepted 13th July 2016

DOI: 10.1039/c6qi00167j

rsc.li/frontiers-inorganic

The use of alkali metal borohydrides for hydrogen storage has long been restricted by high dehydrogenation temperature and large endothermic dehydrogenation enthalpy. Here we report that the dehydrogenation properties of $NaBH_4$ and $LiBH_4$ can be significantly improved by the ionic liquid (IL) 1-butyl-3-methylimidazolium bis(trifluoromethylsulfonyl)imide ($bmimNTf_2$). The borohydrides form homogeneous solutions in $bmimNTf_2$, which release more than 70% of theoretical hydrogen below 180 °C, significantly lower than that in the solid state (370 °C for $LiBH_4$ and 500 °C for $NaBH_4$). The dehydrogenation reactions become highly exothermic in the IL, which is in contrast to the highly endothermic process in their solid states. The drastically changed dehydrogenation behaviour in IL is attributed to the destabilization of borohydrides due to the more favorable charge transfer from BH_4^- to the cation in the IL, which is in line with the established stability rule of metal borohydrides. The IL remains unchanged after dehydrogenation, which provides the possibility of its repeated use.

Introduction

Hydrogen is an outstanding next-generation energy source for its abundance, cleanliness and high energy capacity. However, safe and compact storage of hydrogen has long been a crucial and restrictive step in the widespread use of hydrogen energy.[1–3] For on-board applications, many properties including gravimetric/volumetric capacity, (de)hydrogenation thermodynamics and kinetics and reversibility should be considered. Researchers have investigated many hydrogen storage materials such as metal hydrides,[4] borohydrides,[5] amides/imides,[6] alanates,[7] ammonia borane (AB)[8] and their combinations.[9] Unfortunately, these solid state materials or their combinations can hardly meet the requirement of practical application.

Alkali metal borohydrides are promising candidates for hydrogen storage due to their high gravimetric hydrogen capacity ($LiBH_4$, 18.5 wt%; $NaBH_4$, 10.7 wt%). However, the use of these compounds through thermal dehydrogenation is predominantly hindered by the extraordinarily high dehydrogenation temperature.[10,11] This drawback mainly originates from the high dehydrogenation enthalpy of alkali metal borohydrides, *i.e.*, the strong endothermic effect during dehydrogenation (Table 1). Therefore, modifying the dehydrogenation enthalpy by either destabilizing the reactants or stabilizing the products is a crucial and effective way to lower the dehydrogenation temperature.

There are many examples of the "stabilizing the products" strategy. By adding hydrides and/or other borohydrides containing alkali-earth or transition metals, stable borides can form, which significantly decreases the dehydrogenation enthalpy and lowers the dehydrogenation temperature. For instance, in the dehydrogenation reaction of a $LiBH_4 + MgH_2$ composite, a more stable phase, MgB_2, is formed as the final product.[12] As a result, the dehydrogenation temperature is lowered to 270 °C. In another example, $LiBH_4$ is ball-milled with CaH_2 and forms CaB_6 as the final product upon dehydrogenation.[13] Many similar composites are investigated including $LiBH_4 + CeH_2$,[13] $LiBH_4 + Ca(BH_4)_2$,[14] $NaBH_4 + MgH_2$,[15] $NaBH_4$–CaH_2/$Ca(BH_4)_2$,[16] $LiBH_4 + TiF_3$,[17] $LiBH_4 + AlF_3$,[18] $NaBH_4$–YH_3,[19] *etc.* Although the "stabilizing the product" strategy shows certain effectiveness, the dehydrogenation temperature of most of these composites remains very high (typically >300 °C), with a dehydrogenation enthalpy larger than 40 kJ mol^{-1} H_2. Moreover, the introduced additives significantly lower the hydrogen content and often cause complicated side reactions and formation of by-products.

An alternative strategy is to destabilize the reactants. This strategy requires thermodynamic modification on the borohydrides themselves. It is more difficult to apply as the thermodynamic stability of solid borohydrides is dominated by their intrinsic properties. High-energy ball-milling might cause some destabilization effects by introducing more defects. But

[a]*Beijing National Laboratory for Molecular Sciences (BNLMS), College of Chemistry and Molecular Engineering, Peking University, Beijing, China.*
E-mail: zhengjie@pku.edu.cn, xgli@pku.edu.cn
[b]*Academy for Advanced and Interdisciplinary Studies (AAIS), Peking University, Beijing, P. R. China*

†Electronic supplementary information (ESI) available: Additional figures including illustrations, calibration curves, energetic diagrams, detailed NMR spectra and characterization of precipitations. See DOI: 10.1039/c6qi00167j

Table 1 Dehydrogenation enthalpy and temperature of hydrogen storage materials containing alkali metal borohydride

Reactant	Product	T_d (°C)	$\Delta_r H$ (kJ mol^{-1} H_2)	Ref.
$NaBH_4$	$Na + B + 2H_2$	534[a]	123,[b] 106.8	10 and 31
$NaBH_4$	$NaH + B + 3/2H_2$	—	133.32[b]	10
$LiBH_4$	$LiH + B + 3/2H_2$	370[a]	67,[b] 74	11 and 12
$2LiBH_4 + MgH_2$	$2LiH + MgB_2 + 4H_2$	270	40.5	15
$6LiBH_4 + CaH_2$	$6LiH + CaB_6 + 10H_2$	350	59	32
$2NaBH_4 + MgH_2$	$2Na + MgB_2 + 5H_2$	515	90.9	15 and 31
$3LiBH_4 + TiF_3$	$3LiF + TiB_2 + B + 6H_2$	269	−157.1	17
$3NaBH_4 + YF_3$	$3NaF + 3/4YB_4 + 1/4YH_2 + 23/4H_2$	423	51.2	19
$NaBH_4$ (in IL)	$NaBH_{1.04} + 1.48H_2$	179	−183.0	This work
$LiBH_4$ (in IL)	$LiBH_{1.16} + 1.42H_2$	162	−138.3	This work

[a] These dehydrogenation temperatures are given by the extrapolation of the Van't Hoff plot. [b] These reaction enthalpies are calculated using the thermodynamic data of reactants and products.

the experimental investigation on ball-milled $NaBH_4$–MgH_2 and $LiBH_4$–MgH_2 composites shows little improvement in terms of both the dehydrogenation temperature and thermodynamics.[20,21]

Here we report a novel approach to destabilize the alkali borohydrides $NaBH_4$ and $LiBH_4$ by dissolving the borohydrides into an ionic liquid (IL). There have been a few studies on using ILs for hydrogen storage. The IL methylguanidinium borohydride has been studied as a hydrogen storage material dissolved in ethylene diglyme.[22] In this case, the IL behaves just like other solid borohydrides, which is catalytically decomposed to give hydrogen and a solid product. Imidazolium-based ILs have been shown to have a catalytic effect on dehydrogenation from ammonia borane (AB)[23–25] and ethylene diaminebisborane (EDB).[26] However, as the dehydrogenation of AB and EDB is thermodynamically favourable, similar or even better promotion effects can also be achieved by a large variety of solid catalysts.[27,28]

For the thermodynamically highly stable alkali metal borohydrides, the effect of IL on the dehydrogenation is more drastic and unique. Dissolving in IL significantly lowers the dehydrogenation temperature and completely reverses dehydrogenation thermodynamics. Interestingly, $NaBH_4$ and $LiBH_4$ exhibit very similar dehydrogenation behaviour in the IL. Over 70% of theoretical hydrogen can be released from 160–180 °C. Moreover, the IL shows no structural changes after dehydrogenation and can be easily recycled, behaving as a pure catalyst in the very classic definition. The favourable dehydrogenation temperature of the liquid borohydride-IL hydrogen storage system will greatly advance the application of borohydrides as high capacity hydrogen storage materials.

Experimental section

Synthetic procedure

Materials. $NaBH_4$ (99.5%) and $LiBH_4$ (99.5%) are purchased from J&K Chemical Co. Ltd. 1-Butyl-3-methylimidazolium bromide (bmimBr), 1-butyl-2,3-dimethylimidazolium bromide (bmmimBr) and lithium bis(trifluoromethylsulfonyl)imide ($LiNTf_2$) are purchased from Lanzhou Institute of Chemistry and Physics. All the materials are used as-received unless stated otherwise.

Synthesis of bmimNTf$_2$ and bmmimNTf$_2$. BmimBr (12.98 g, 59 mmol) and $LiNTf_2$ (17.02 g, 59 mmol) are dissolved in 100 mL of deionized water respectively. Then the two clear solutions are mixed in a 500 mL flask, which rapidly develops a water–oil interface. The oil phase is separated and washed six times with deionized water until it becomes clear. The IL is extracted by dichloromethane, thoroughly washed with water three times and distilled under vacuum to remove dichloromethane. The IL is further kept at 120 °C for 4 days under dynamic vacuum and then transferred into an Ar-filled glovebox. The IL is characterized by using ^{1}H NMR. No residual water is detected on the NMR spectrum (Fig. 1a and d). The ionic structure of the $bmimNTf_2$ is shown in Fig. 1c. 1-Butyl-2,3-dimethylimidazolium bis(trifluoromethylsulfonyl)imide

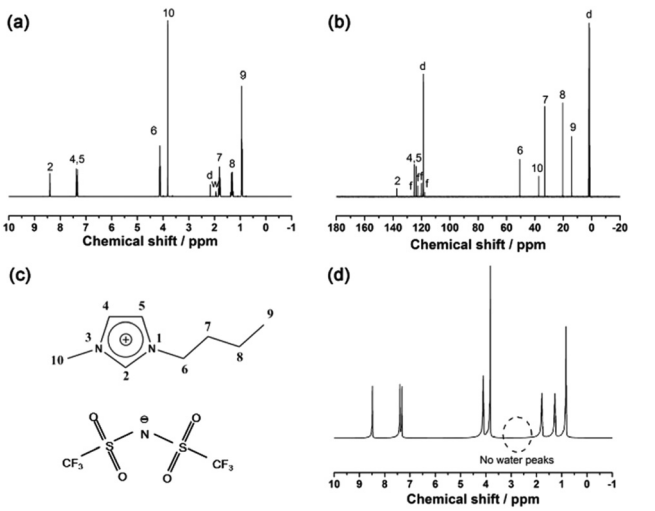

Fig. 1 (a) ^{1}H NMR spectrum of the as-prepared $bmimNTf_2$ sample in CD_3CN. (b) ^{13}C NMR spectrum of the as-prepared $bmimNTf_2$ sample in CD_3CN. The digits in (a) and (b) are corresponding to the atoms labelled in (c). The letters d, w and f represent CD_3CN, water and trifluoromethyl, respectively; (c) ionic structure of $bmimNTf_2$; (d) ^{1}H NMR spectrum of the as-prepared $bmimNTf_2$ sample without deuterated solvent.

($bmmimNTf_2$) is synthesized in the same way using bmmimBr (13.44 g, 58 mmol) and $LiNTf_2$ (16.56 g, 58 mmol).

Preparation of borohydride-IL samples. $NaBH_4$ (11.0 mg, 0.29 mmol) and $bmimNTf_2$ (11.99 g, 29 mmol) are milled in an agate mortar for 20 min to form a clear, colorless solution. The samples of $bmimNTf_2$-$LiBH_4$-1 mol% (denoted as $LiBH_4$-IL), $bmmimNTf_2$-$NaBH_4$-1 mol% (denoted as $NaBH_4$-$bmmimNTf_2$) and $bmmimNTf_2$-$LiBH_4$-1 mol% (denoted as $LiBH_4$-$bmmimNTf_2$) are prepared and stored using the same procedure. All these samples are clear and colourless solutions with relatively high viscosity. All the samples are prepared and stored in an Ar-filled glovebox.

Preparation of bmimBr/$LiNTf_2$–borohydride samples. BmimBr and $LiNTf_2$ are held at 150 °C under dynamic vacuum for 24 h to remove water before use. The bmimBr-$NaBH_4$-1 mol% sample (denoted as bmimBr-$NaBH_4$) is prepared by milling $NaBH_4$ (10.5 mg, 0.28 mmol) and bmimBr (5.99 g, 27.4 mmol) in an agate mortar for 15 min. The sample is collected and stored in a glass bottle. The samples of bmimBr-$LiBH_4$-1 mol% (denoted as bmimBr-$LiBH_4$), $LiNTf_2$–$NaBH_4$-1 mol% (denoted as $LiNTf_2$–$NaBH_4$) and $LiNTf_2$–$LiBH_4$-1 mol% (denoted as $LiNTf_2$–$LiBH_4$) are prepared using the same method. They are all white and fine powders. All the samples are prepared and stored in an Ar-filled glovebox.

Characterization techniques

NMR spectroscopy. ^{11}B NMR spectra are collected for liquid samples on a Bruker AVANCE III 500 MHz (for ^1H nuclei) spectrometer. All the ^{11}B NMR data is referenced to $BF_3{\cdot}Et_2O$ (at 0 ppm) as an external standard material. ^1H and ^{13}C NMR spectra are recorded on the same spectrometer. All the NMR spectra are collected in acetonitrile-d_3 unless stated otherwise.

Temperature programmed desorption/mass spectrometry (TPD/MS) analysis. TPD/MS experiments are performed on a Quantachrome Autosorb iQ automatic gas sorption analyser. On heating, the carrier gas (Ar, purity >99.999%) flows through the sample tube and brings the released gas with it. The gas composition is further analysed by a Pfeiffer PrismaPlus™ Mass Spectrometer-Residual Gas Analyser (MS-RGA). Two needle valves, a vent sampling valve and a mass spectrometer input valve, are adjusted to introduce an appropriate amount of gas into the mass spectrometer. The multiple ion detection (MID) mode is used to analyse the temporal variation of the specific products. Temperature is simultaneously measured by a thermocouple installed next to the sample cell. The heating rate is 5 K min^{-1} for all the samples. A gross leak test is performed before each experiment.

Quantification of the hydrogen released. Quantification experiments are performed on a Quantachrome Autosorb iQ automatic gas sorption analyser. A home-made glass tube is used as a container for the liquid sample (Fig. S1, ESI†). The sample is heated in a high purity argon (99.999%) flow of 50 mL min^{-1}. The generated gas is allowed to pass a cold trap cooled by using an ice bath before entering the sampling TCD and the thermal conductivity difference is measured to determine the quantity of the released gas. The acquired TCD signals are integrated to calculate the amount of hydrogen released. The coefficient used to convert the integration to the amount of hydrogen is determined by regression of the working curve using the external standard, pure MgH_2 (Fig. S2, ESI†). For all the measurement runs in this paper, no residue is found in the cold trap. Temperature is simultaneously measured by a thermocouple installed next to the sample cell. The heating rate is 5 K min^{-1} for all the samples. A gross leak test is performed before each experiment.

Differential scanning calorimetry (DSC) measurements. DSC measurements are carried out on a Netzsch DSC HP 204 calorimeter. The sample (15.0 to 25.0 mg) is loaded in an aluminium crucible in an argon-filled glovebox. Another blank crucible is used as the reference. An aluminium lid with a pinhole on it covers the crucible, allowing the gaseous product to escape. The experiments are performed in an inert gas flow (high purity argon, 99.999%, 50 mL min^{-1}, 1.0 bar) with various heating rates.

Results and discussion

Characterization of $bmimNTf_2$ and the borohydride-$bmimNTf_2$ solution

The structure of the as-prepared $bmimNTf_2$ sample is investigated by ^1H and ^{13}C NMR spectra (Fig. 1a and b). The resonance peaks on these spectra can be ascribed to the corresponding H and C atoms in the ion structure shown in Fig. 1c. However, a small resonance peak corresponding to water is found in the ^1H NMR spectrum. To find out whether this water residue is from $bmimNTf_2$ or deuterated solvent, we performed a ^1H NMR experiment of pure $bmimNTf_2$ without deuterated solvent (Fig. 1d). No peaks related to water are found in these spectra. Therefore, these results proved that the $bmimNTf_2$ prepared is pure and dry. Therefore, it can be used in the follow-up experiments.

After milling, the mixtures of MBH_4 and IL are clear and colourless solutions, as shown in Fig. 2b. The disappearance of borohydride solids during milling indicates dissolution of borohydrides in $bmimNTf_2$. The ^1H NMR spectra of $NaBH_4$-IL and $LiBH_4$-IL samples are shown in Fig. 2a. The multiplets from −0.5 to 0.5 ppm prove the existence of BH_4^- anions in the samples. In the ^{11}B NMR spectra (Fig. 2b), the quintets

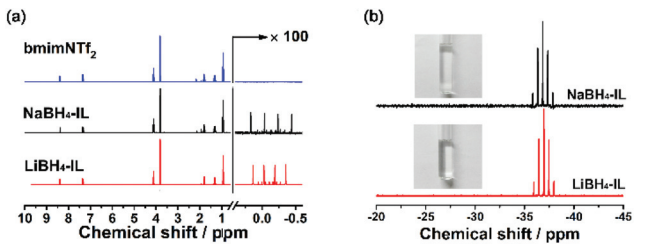

Fig. 2 (a) ^1H NMR spectra of pristine $bmimNTf_2$, $NaBH_4$-IL and $LiBH_4$-IL samples; (b) ^{11}B NMR spectra of the $NaBH_4$-IL and $LiBH_4$-IL samples. The inset pictures are the photographs of the corresponding samples.

centred at −37.0 and −36.8 ppm can be ascribed to the resonance signals of BH_4^- in the samples. These spectroscopic features are very similar to those of BH_4^- in the solid state and other solvents.[29,30]

Furthermore, in both ^1H (Fig. 2a) and ^{13}C NMR spectra of $NaBH_4$-IL and $LiBH_4$-IL samples (Fig. S3, ESI†), the resonance peaks corresponding to $bmimNTf_2$ do not change, indicating that the structure of IL does not change after dissolution of the borohydrides. These results indicate that the borohydrides can be dissolved into the IL without changing the structure of the IL or BH_4^- during the milling procedure.

Dehydrogenation properties

Fig. 3a and b show the dehydrogenation profile of $NaBH_4$-IL and $LiBH_4$-IL monitored by TPD/MS, respectively. The onset dehydrogenation temperature is 104 °C for $NaBH_4$-IL and 85 °C for $LiBH_4$-IL, while the peak temperature is 179 °C for $NaBH_4$-IL and 162 °C for $LiBH_4$-IL, respectively. No gaseous impurities are found under these conditions. The IL decomposes and emits some gaseous impurities above 200 °C. To avoid the decomposition of IL, the dehydrogenation temperature is limited to 180 °C for $NaBH_4$ and 160 °C for $LiBH_4$, respectively.

Fig. 3c and d show the amount of H_2 released from both samples determined by TCD measurement. For the $NaBH_4$-IL sample, the dehydrogenated hydrogen content is 8.1% based on $NaBH_4$, covering 74% of the hydrogen in $NaBH_4$. For the $LiBH_4$-IL sample, the dehydrogenated content is 13.2 wt% based on $LiBH_4$, covering 71% of the hydrogen in $LiBH_4$. At the dehydrogenation temperature of $NaBH_4$-IL and $LiBH_4$-IL samples, the solid state $NaBH_4$ and $LiBH_4$ show no evidence of dehydrogenation. Such dehydrogenation properties are definitely not from a hydrolysis reaction since no residual water is detected in $bmimNTf_2$ (Fig. 1d).

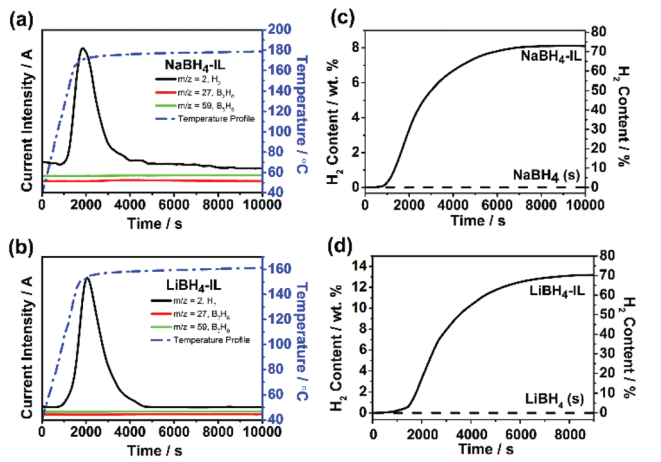

Fig. 3 TPD/MS curves of $NaBH_4$-IL (a) and $LiBH_4$-IL (b) samples in their dehydrogenation reaction. The MS signals for H_2 (m/z = 2, black), B_2H_6 (m/z = 27, red), and B_5H_9 (m/z = 59, green) are demonstrated in solid lines. The blue dashed curves show the temperature profile; isothermic dehydrogenation profiles of $NaBH_4$-IL (c) and $LiBH_4$-IL (d). For comparison, the hydrogen released at the same temperature from solid $NaBH_4$ and $LiBH_4$ is also shown.

The dehydrogenation products

After dehydrogenation, the samples appear as a clear solution with some precipitates at the bottom of the reaction tube. The solution is studied using ^{11}B, ^1H and ^{13}C NMR spectra. ^{11}B NMR spectra of the solution indicate that the BH_4^- anion in borohydrides completely decomposes in the dehydrogenation reaction (Fig. 4a and b), which is in agreement with the absence of the B–H resonance peak in the ^1H NMR spectra in the 0.5 to −0.5 ppm region (Fig. 4c). The full range ^{11}B NMR spectra are shown in Fig. S4 (see the ESI†), showing no soluble boron-containing species in the solution phase. It means that all the boron-containing species are enriched in the solid phase.

Regarding the structure of IL after dehydrogenation, the ^1H NMR (Fig. 4c) spectra suggest that the chemical bonding of H atoms is not changed by heating or chemical reactions. Meanwhile, no evidence for the formation of C–B bonds or any other new C-related bonds is found in ^{13}C NMR spectra (Fig. 4d). The above results indicate that the IL $bmimNTf_2$ is chemically stable and serves as a pure solvent in the dehydrogenation. Therefore, we may conclude that the dehydrogenated samples consist of a boron-containing solid phase and a liquid phase of pure IL. The stability of the IL during dehydrogenation makes recycling of the IL after dehydrogenation for repeated use possible.

The precipitate is also characterized using XRD (Fig. S5, ESI†) and FT-IR (Fig. S6, ESI†). The XRD patterns show broad peaks for both $NaBH_4$-IL and $LiBH_4$-IL samples, indicating that the dehydrogenation products are amorphous. In the IR spectra, only very weak peaks are detected in the B–H stretching region (2250–2400 cm^{-1}), indicating little residual B–H bond in the dehydrogenation products. This indicates rather complete elimination of the B–H bonds at moderate

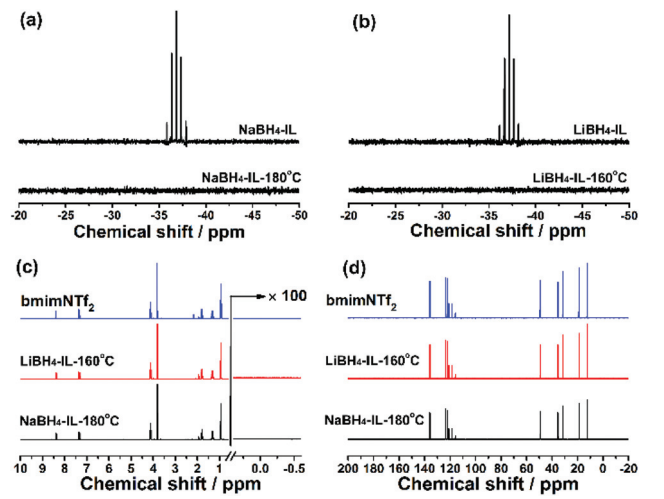

Fig. 4 ^{11}B NMR spectra of the $NaBH_4$-IL (a) and $LiBH_4$-IL (b) samples before and after dehydrogenation. ^1H NMR (c) and ^{13}C NMR (d) spectra of pristine $bmimNTf_2$ and dehydrogenated samples. The ^{13}C NMR spectra are recorded without deuterated solvents.

temperature in IL. According to the dehydrogenation capacity (Fig. 3c and d), the nominal dehydrogenation reaction of $NaBH_4$-IL and $LiBH_4$-IL can be described by eqn (1) and (2), respectively.

$$NaBH_4\text{-IL} \rightarrow NaBH_{1.04} + IL + 1.48H_2 \quad (1)$$

$$LiBH_4\text{-IL} \rightarrow LiBH_{1.16} + IL + 1.42H_2 \quad (2)$$

In their solid states, borohydrides usually exhibit multiple dehydrogenation steps. A stable intermediate species, $M_2B_{12}H_{12}$, is found to be the key intermediate in the dehydrogenation reaction pathway of alkali metal borohydrides.[33–35] However, in MBH_4-IL samples, the dehydrogenation capacity is much higher (70–75%) compared to the partial dehydrogenation of MBH_4 to $M_2B_{12}H_{12}$. The stoichiometry of the dehydrogenation products in the IL cannot be attributed to any known alkali metal hydroborates. Rather, it best matches a mixture of boron and metal hydride, which is the dehydrogenation product at high temperature for solid state $LiBH_4$ and $NaBH_4$.[10,11] This is also in agreement with the very low residual B–H bonding in the solid precipitate. Further characterization of the solid dehydrogenation product will be our next research focus.

Another interesting observation is the highly similar dehydrogenation behaviour in terms of both dehydrogenation temperature and the dehydrogenation capacity of $NaBH_4$-IL and $LiBH_4$-IL. In the solid state, there is a significant difference in the dehydrogenation temperature and dehydrogenation mechanism.[5] The nearly metal independent dehydrogenation behaviour has important implications for the dehydrogenation mechanism, as will be discussed later.

Thermodynamic and kinetic investigation

Since the dehydrogenation temperatures of borohydride-IL samples are far lower than those calculated from thermodynamic parameters of solid state materials, the thermodynamic property of this system is very interesting. Therefore, we perform DSC measurements to compare the thermodynamic behaviour of $NaBH_4$ and $LiBH_4$ in IL and their solid states. In their crystalline states, $NaBH_4$ and $LiBH_4$ show very strong endothermic behaviour during dehydrogenation at high temperature (370 °C for $LiBH_4$ and 500 °C for $NaBH_4$) (Fig. 5b and d). The solid state $LiBH_4$ experiences an orthorhombic to tetragonal phase change (~130 °C) and melting (~280 °C) before dehydrogenation.[36] The dehydrogenation enthalpy is reported to be 108 kJ mol^{-1} and 74 kJ mol^{-1} for pristine $NaBH_4$ and $LiBH_4$, respectively.[10,11]

Surprisingly, the dehydrogenation of $NaBH_4$-IL and $LiBH_4$-IL samples becomes highly exothermic (Fig. 5a and c). The $NaBH_4$-IL sample exhibits an exothermic peak at 134 °C, and the dehydrogenation enthalpy is −183.0 kJ mol^{-1} H_2. The $LiBH_4$-IL sample also shows an exothermic peak at 127 °C, and the dehydrogenation enthalpy is −138.3 kJ mol^{-1} H_2. In contrast to their very similar dehydrogenation temperature and dehydrogenation capacity, the dehydrogenation enthalpy of $NaBH_4$-IL and $LiBH_4$-IL is quite different. The dehydrogenation

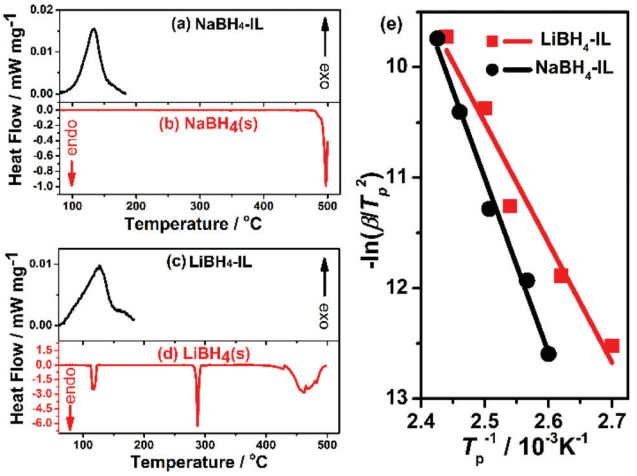

Fig. 5 DSC curves of $NaBH_4$-IL and solid state $NaBH_4$ (a, b) and $LiBH_4$-IL and solid state $LiBH_4$ (c, d) at a heating rate of 2 K min^{-1}. The Kissinger's plots of $NaBH_4$-IL (black) and $LiBH_4$-IL (red) are demonstrated in (e). The apparent activation energy (E_a) is calculated from the slope of the fitted lines (the solid lines) according to the Kissinger's equation (eqn (3)).

enthalpies are lower than those in most of the systems listed in Table 1,[12,15,31,32] but are similar to those observed in the borohydride–fluoride composites like $LiBH_4$–YF_3,[17] which has an exothermic dehydrogenation enthalpy due to the formation of highly thermodynamically stable products such as LiF and TiB_2. However, the exothermic dehydrogenation is rather surprising for MBH_4-IL, as the IL is unchanged after dehydrogenation. The favourable dehydrogenation of MBH_4-IL, therefore, is a result of destabilized reactants. It is a much advantageous approach because no reactive additives are involved in the dehydrogenation reaction.

The activation energy of the dehydrogenation process is evaluated using the Kissinger's equation by measuring multiple DSC curves (Fig. S7 and S8, ESI†) at different heating rates (eqn (3)).[37]

$$\frac{d\left(\ln\frac{\beta}{T_p^2}\right)}{d\left(-\frac{1}{T_p}\right)} = \frac{E_a}{R}, \quad (3)$$

where β is the heating rate of DSC measurements (K min^{-1}), T_p is the peak temperature on the DSC curve, R is the ideal gas constant and E_a is the apparent activation energy.

The apparent activation energies for $NaBH_4$-IL and $LiBH_4$-IL samples are calculated to be 131.3 kJ mol^{-1} and 91.4 kJ mol^{-1}, respectively (Fig. 5e). The high apparent activation energy shows that both $NaBH_4$-IL and $LiBH_4$-IL are thermodynamically unstable systems stabilized by kinetic barriers. It also provides the possibility to further lower the dehydrogenation temperature by introducing suitable catalysts in the MBH_4-IL system, which will be a very interesting field deserving further exploration.

Dehydrogenation mechanism study

Destabilization of MBH_4 by IL. According to the DSC results, dehydrogenation of the solid state MBH_4 (or melted $LiBH_4$) is highly endothermic:

$$\Delta_r H(MBH_4, s) = \Delta_f H(MBH) - \Delta_f H(MBH_4, s) > 0 \quad (4)$$

The solid dehydrogenation product is represented by "MBH", which can be considered as a mixture of metal hydride and elemental boron, the high temperature dehydrogenation product of $NaBH_4$ and $LiBH_4$.

In contrast, DSC results also suggest that dehydrogenation of MBH_4 in the IL (eqn (1) and (2)) is highly exothermic:

$$\Delta_r H(MBH_4\text{-IL}) = \Delta_f H(MBH) + \Delta_f H(IL) - \Delta_f H(MBH_4\text{-IL}) < 0 \quad (5)$$

Here the solid dehydrogenation product precipitated from the IL is also represented by "MBH", according to the stoichiometry derived from the dehydrogenation capacity. The term $\Delta_f H(MBH_4\text{-IL})$ describes the formation enthalpy of the MBH_4-IL samples. This term can be approximated as the sum of the inherent formation enthalpy of IL ($\Delta_f H(IL)$) and the energy of the dissolved MBH_4 ($\Delta_f H(MBH_4$ in IL)).

$$\Delta_f H(MBH_4\text{-IL}) \approx \Delta_f H(MBH_4 \text{ in IL}) + \Delta_f H(IL) \quad (6)$$

This is a rather good approximation for a dilute MBH_4-IL solution. In this case we can treat the IL as an infinitely large bath which is little affected by the dissolved borohydrides.

According to eqn (4), (5), and (6), the borohydride in IL becomes less stable compared to that in the solid state (eqn (7)),

$$\Delta_f H(MBH_4 \text{ in IL}) \gg \Delta_f H(MBH_4, s) \quad (7)$$

Both $NaBH_4$ and $LiBH_4$ are typical ionic crystals.[38,39] Using the gas phase ions $M^+(g)$ and $BH_4^-(g)$ as the reference state, $\Delta_f H(MBH_4, s)$ is virtually the lattice enthalpy of MBH_4 (ΔU_{MBH_4}). On the other hand, $\Delta_f H(MBH_4$ in IL) is the solvation enthalpy (E_s) in the IL, determined by the interaction between the borohydrides and the IL. The destabilization effect (eqn (7)), therefore, is a result of the large difference between ΔU_{MBH_4} and E_s:

$$\Delta_f H(MBH_4 \text{in IL}) - \Delta_f H(MBH_4, s) = E_{s,MBH_4\text{-IL}} - \Delta U_{MBH_4} \gg 0 \quad (8)$$

The energetics of the M–B–H species are summarized in Scheme 1. In this diagram, two approximations are made except that in deriving eqn (6): (1) in the case of pristine $LiBH_4$, we neglect the energy change due to phase transition and melting. However, these terms are small compared to the lattice enthalpy of $LiBH_4$ and can be included as a slight upshift of the position of $LiBH_4$ in the energy diagram. (2) We use the same dehydrogenation product "MBH" for both pristine MBH_4 and MBH_4-IL. This could be complicated by other dehydrogenation products, particularly in the case of low temperature dehydrogenation in the solid state. Nevertheless,

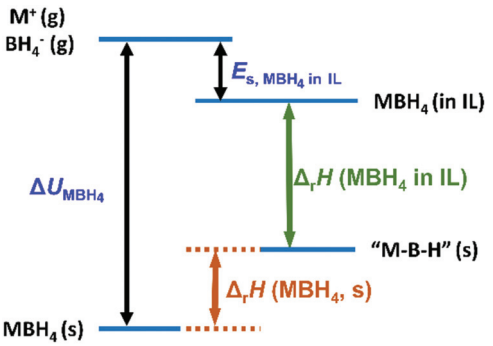

Scheme 1 A schematic energy diagram of the dehydrogenation of borohydrides in the solid state and IL solution.

the MBH_4 is the most stable M–B–H species compared to all the dehydrogenation products composed of M–B–H. For instance, one well known stable dehydrogenation intermediate $M_2B_{12}H_{12}$ is also an endothermic product from MBH_4.[34] Therefore, other M–B–H type solid state dehydrogenation products can be regarded as a band around the representative "MBH" species.

The above approximations may cause slight adjustments on the energetic diagram, as shown in Fig. S9 (see the ESI†). However, the simplified diagram (Scheme 1) is sufficiently illustrative. The stability increases in the order: MBH_4 in IL < the dehydrogenation product (represented by "MBH") < MBH_4(s), as suggested by the DSC results. This diagram clearly shows that the reversed dehydrogenation thermodynamics in the IL is caused by destabilization of MBH_4. This diagram also explains the limitation of thermodynamic modulation in the solid state. In pristine MBH_4, the thermodynamics is dominated by the large lattice enthalpy (ΔU_{MBH_4}). Consequently, the dehydrogenation is always highly endothermic for M–B–H type products, as suggested by previous studies.[34,40]

The interaction between BH_4^- and the cation in the IL. The destabilization of MBH_4 in IL is due to the interaction between the borohydrides and the IL. To understand this interaction, we study the effect of the cation and the anion in the IL separately (Fig. 6). The bmimBr-$NaBH_4$ and bmimBr-$LiBH_4$ samples

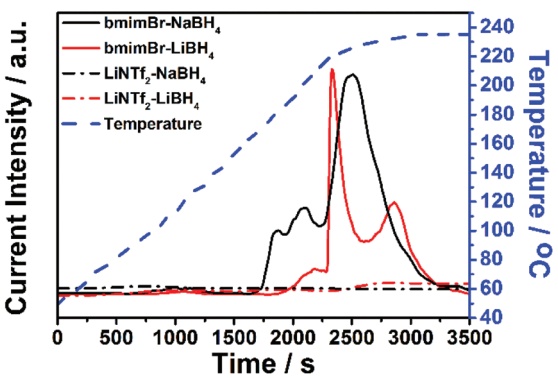

Fig. 6 TPD curves of bmimBr-$NaBH_4$ (black, solid), bmimBr-$LiBH_4$ (red, solid), $LiNTf_2$–$NaBH_4$ (black, dash dot) and $LiNTf_2$–$LiBH_4$ (red, dash dot) samples. The temperature profile is demonstrated as blue dashed line.

dehydrogenate at 220 and 230 °C, respectively, which are also significantly lower than those in the solid state and only slightly higher than those of the corresponding MBH_4-IL samples. On the other hand, both $LiNTf_2$–borohydride composites show negligible dehydrogenation under 240 °C, as shown in Fig. 6. The above results suggest that $bmim^+$ is the active component in the IL responsible for the promoted dehydrogenation properties of the borohydrides while NTf_2^- is ineffective.

At this stage, it is illustrative to recall the highly similar dehydrogenation temperature and capacity for $LiBH_4$ and $NaBH_4$ in the IL (Fig. 3), while a large difference is observed in their solid states. In dilute IL solution of borohydrides, BH_4^- is mostly surrounded by $bmim^+$ cations rather than the metal cations. The almost cation independent dehydrogenation temperature and capacity, therefore, are a natural consequence of the new dehydrogenation mechanism in IL, *i.e.*, dehydrogenation dominated by the $bmim^+/BH_4^-$ interaction.

Destabilization of borohydrides due to the $bmim^+/BH_4^-$ interaction is in well accordance with the stability rule observed in solid metal borohydrides.[41] Nakamori *et al.* reported that the stability of borohydride is determined by the electronegativity of the metal in the metal borohydride. Metals with lower electronegativity (*e.g.* alkali metals) form more stable borohydrides.[42] This rule is well explained by charge transfer between BH_4^- and metal cations.[41,43] Charge transfer from BH_4^- to the cations will lower the negative charge on BH_4^- and consequently destabilize the borohydride. In alkali metal borohydride such as $NaBH_4$ and $LiBH_4$, an ionic picture has been proposed by *ab initio* calculations.[39] The charge on the alkali metal cation is close to +1. In stable borohydrides such as $LiBH_4$, $NaBH_4$ and $Ca(BH_4)_2$, the charge transfer between M^{n+} and BH_4^- is relatively low, while in unstable borohydrides such as $Zn(BH_4)_2$ and $CuBH_4$, the charge transfer is relatively large.[44]

The charge transfer strongly depends on the nature of the cation. Cations that are more inclined to accept negative charges favour the charge transfer and consequently destabilize the borohydride. For simple metal cations, this trend can be well described by the electronegativity of the corresponding metal. In our study, $bmim^+$ is a large cation with a conjugated system. Such a structure is more favourable to accommodate extra negative charges, as the electron delocalization effect can stabilize the extra electron density. Indeed, both experimental and theoretical studies suggest that there is a notable charge transfer effect from NTf_2^- to $bmim^+$ in $bmimNTf_2$ or similar ILs.[45] Such a charge transfer effect is expected to be more favourable from the less electron pulling BH_4^- (compared to NTf_2^-). Therefore, the $bmim^+/BH_4^-$ interaction destabilizes the BH_4^- due to the enhanced electron transfer to $bmim^+$, which explains the significantly lower dehydrogenation temperature and exothermic nature of the dehydrogenation process.

To further verify the charge transfer based destabilization mechanism, the dehydrogenation of borohydrides in another IL $bmmimNTf_2$ (bmmim = 1-butyl-2,3-dimethylimidazolium) is studied. The cation $bmmim^+$ differs from $bmim^+$ by the methyl group on the 2-C of the imidazolium ring. The 2-H in $bmim^+$ may be deprotonated by strong bases. Methyl substitution eliminates this potentially active H species. Fig. 7 shows the TPD/MS curves of $NaBH_4$-$bmmimNTf_2$ and $LiBH_4$-$bmmimNTf_2$ samples. They show a very similar dehydrogenation temperature to that of $NaBH_4$-$bmimNTf_2$ and $LiBH_4$-$bmimNTf_2$ samples. Destabilization of BH_4^-, therefore, is not associated with the 2-H of $bmim^+$. Furthermore, this result can be well explained by the charge transfer mechanism, as the methyl substitution for H has little effect on the electron affinity of the imidazolium cation. The bulky imidazolium cation with the conjugated structure may stabilize an extra negative charge and thus cause more favourable charge transfer from BH_4^-, which is little affected by the alkyl groups on the imidazolium ring.

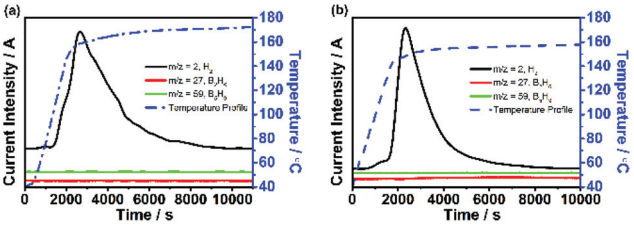

Fig. 7 TPD/MS curves of $NaBH_4$-$bmmimNTf_2$ (a) and $LiBH_4$-$bmmimNTf_2$ (b) samples. The MS signals for H_2 (m/z = 2, black), B_2H_6 (m/z = 27, red), and B_5H_9 (m/z = 59, green) are demonstrated in solid lines. The blue dashed lines show the temperature profile of the dehydrogenation reaction.

The MBH_4-IL system represents a new type of liquid hydrogen storage system. Similar to the well-studied liquid organic hydrogen storage systems,[46,47] the MBH_4-IL shares many advantages in transport, storage and handling arising from the liquid form. Liquid hydrogen storage systems based on ILs are rare but not totally absent. Previous reports show that ILs can promote the dehydrogenation kinetics of B–N–H type compounds such as NH_3BH_3 and $BH_3NH_2CH_2CH_2NH_2BH_3$.[23–26] However, as the first step dehydrogenation of these materials is thermodynamically favourable, the role of the IL is mainly a kinetic promoter and toxic gas inhibitor. In fact, similar or even better promotion effects have also been achieved by many other solid catalysts.[8,27]

On the other hand, the role of the IL for $LiBH_4$ and $NaBH_4$ is truly unique and indispensable. The promotion effect in terms of dehydrogenation temperature is unrivalled by any other additive reported so far. The strong ion pair interaction in MBH_4-IL dramatically changes the dehydrogenation temperature and thermodynamics of the borohydrides, which is an important advantage towards the application of $NaBH_4$ and $LiBH_4$ as high capacity hydrogen storage materials. Although inclusion of IL reduces the hydrogen capacity in one dehydrogenation cycle, repeated use of the IL is possible as the IL is unaffected during the dehydrogenation and can be easily separated from the solid state dehydrogenation residue. With engineering efforts to recycle the IL, high hydrogen capacity is attainable for the MBH_4-IL system.

Conclusions

The dehydrogenation of alkali metal borohydrides $NaBH_4$ and $LiBH_4$ in the ionic liquid $bmimNTf_2$ is studied. Three important observations are noted. (1) The dehydrogenation in IL occurs at 160–180 °C, which is similar for $NaBH_4$-IL and $LiBH_4$-IL and is much lower than that in their solid states. (2) The dehydrogenation process in the IL is strongly exothermic while it is endothermic in the solid state. (3) The IL remains unaffected after the dehydrogenation process and can be easily separated from the solid dehydrogenation residue of the borohydrides.

The distinct dehydrogenation behaviour originates from the interaction between BH_4^- and the cation in the IL which destabilizes BH_4^-. The destabilization mechanism involves a more favourable charge transfer from BH_4^- to the bulky imidazolium cation, which is in line with the well-established stability rule of metal borohydrides. The borohydride-IL system is a promising liquid hydrogen storage system with high attainable hydrogen capacity at moderate temperature.

Acknowledgements

This study is supported by National Natural Science Foundation of China (no. U1201241, 11375020, 51431001 and 21321001). The authors acknowledge Prof. Taiwei Chu from Peking University for his assistance in synthesizing the ionic liquids.

Notes and references

1 L. Schlapbach and A. Zuttel, *Nature*, 2001, **414**, 353–358.
2 J. Graetz, *Chem. Soc. Rev.*, 2009, **38**, 73.
3 S.-i. Orimo, Y. Nakamori, J. R. Eliseo, A. Zuettel and C. M. Jensen, *Chem. Rev.*, 2007, **107**, 4111–4132.
4 B. Sakintuna, F. Lamaridarkrim and M. Hirscher, *Int. J. Hydrogen Energy*, 2007, **32**, 1121–1140.
5 A. Zuettel, A. Borgschulte and S.-I. Orimo, *Scr. Mater.*, 2007, **56**, 823–828.
6 P. Chen, Z. T. Xiong, J. Z. Luo, J. Y. Lin and K. L. Tan, *Nature*, 2002, **420**, 302–304.
7 B. Bogdanovic and M. Schwickardi, *J. Alloys Compd.*, 1997, **253**, 1–9.
8 B. Peng and J. Chen, *Energy Environ. Sci.*, 2008, **1**, 479–483.
9 J. H. Luo, X. D. Kang and P. Wang, *Int. J. Hydrogen Energy*, 2013, **38**, 4648–4653.
10 P. Martelli, R. Caputo, A. Remhof, P. Mauron, A. Borgschulte and A. Zuettel, *J. Phys. Chem. C*, 2010, **114**, 7173–7177.
11 P. Mauron, F. Buchter, O. Friedrichs, A. Remhof, M. Bielmann, C. N. Zwicky and A. Zuettel, *J. Phys. Chem. B*, 2008, **112**, 906–910.
12 J. J. Vajo, S. L. Skeith and F. Mertens, *J. Phys. Chem. B*, 2005, **109**, 3719–3722.
13 S.-A. Jin, Y.-S. Lee, J.-H. Shim and Y. W. Cho, *J. Phys. Chem. C*, 2008, **112**, 9520–9524.
14 J. Y. Lee, D. Ravnsbaek, Y.-S. Lee, Y. Kim, Y. Cerenius, J.-H. Shim, T. R. Jensen, N. H. Hur and Y. W. Cho, *J. Phys. Chem. C*, 2009, **113**, 15080–15086.
15 J. F. Mao, X. B. Yu, Z. P. Guo, H. K. Liu, Z. Wu and J. Ni, *J. Alloys Compd.*, 2009, **479**, 619–623.
16 J. F. Mao, Z. P. Guo, X. B. Yu and H. K. Liu, *J. Phys. Chem. C*, 2011, **115**, 9283–9290.
17 Y. H. Guo, X. B. Yu, L. Gao, G. L. Xia, Z. P. Guo and H. K. Liu, *Energy Environ. Sci.*, 2010, **3**, 465–470.
18 P. P. Yuan, B. H. Liu, H. P. Zhu, W. Y. Pan and Z. P. Li, *J. Alloys Compd.*, 2013, **557**, 124–129.
19 J. Zou, L. Li, X. Zeng and W. Ding, *Int. J. Hydrogen Energy*, 2012, **37**, 17118–17125.
20 S. Garroni, C. Pistidda, M. Brunelli, G. B. M. Vaughan, S. Surinach and M. D. Baro, *Scr. Mater.*, 2009, **60**, 1129–1132.
21 K. Crosby and L. L. Shaw, *Int. J. Hydrogen Energy*, 2010, **35**, 7519–7529.
22 A. Doroodian, J. E. Dengler, A. Genest, N. Roesch and B. Rieger, *Angew. Chem., Int. Ed.*, 2010, **49**, 1871–1873.
23 D. W. Himmelberger, L. R. Alden, M. E. Bluhm and L. G. Sneddon, *Inorg. Chem.*, 2009, **48**, 9883–9889.
24 R. K. Ahluwalia, J. K. Peng and T. Q. Hua, *Int. J. Hydrogen Energy*, 2011, **36**, 15689–15697.
25 M. E. Bluhm, M. G. Bradley, R. Butterick, U. Kusari and L. G. Sneddon, *J. Am. Chem. Soc.*, 2006, **128**, 7748–7749.
26 S. Sahler, S. Sturm, M. T. Kessler and M. H. G. Prechtl, *Chem. – Eur. J.*, 2014, **20**, 8934–8941.
27 A. Staubitz, A. P. M. Robertson and I. Manners, *Chem. Rev.*, 2010, **110**, 4079–4124.
28 B. Peng and J. Chen, *Energy Environ. Sci.*, 2008, **1**, 479–483.
29 Y. Yan, A. Remhof, D. Rentsch and A. Zuettel, *Chem. Commun.*, 2015, **51**, 700–702.
30 Y. Yan, A. Remhof, D. Rentsch, Y.-S. Lee, Y. W. Cho and A. Zuettel, *Chem. Commun.*, 2013, **49**, 5234–5236.
31 C. Milanese, S. Garroni, A. Girella, G. Mulas, V. Berbenni, G. Bruni, S. Suriñach, M. D. Baró and A. Marini, *J. Phys. Chem. C*, 2011, **115**, 3151–3162.
32 F. E. Pinkerton and M. S. Meyer, *J. Alloys Compd.*, 2008, **464**, L1–L4.
33 S. J. Hwang, R. C. Bowman, J. W. Reiter, J. Rijssenbeek, G. L. Soloveichik, J. C. Zhao, H. Kabbour and C. C. Ahn, *J. Phys. Chem. C*, 2008, **112**, 3164–3169.
34 Y. Yan, A. Remhof, S.-J. Hwang, H.-W. Li, P. Mauron, S.-i. Orimo and A. Zuettel, *Phys. Chem. Chem. Phys.*, 2012, **14**, 6514–6519.
35 Y. Liu, S. Giri, J. Zhou and P. Jena, *J. Phys. Chem. C*, 2014, **118**, 28456–28461.
36 J. P. Soulie, G. Renaudin, R. Cerny and K. Yvon, *J. Alloys Compd.*, 2002, **346**, 200–205.
37 H. E. Kissinger, *Anal. Chem.*, 1957, **29**, 1702–1706.
38 P. C. Aeberhard, K. Refson and W. I. F. David, *Phys. Chem. Chem. Phys.*, 2013, **15**, 8081–8087.

39 Z. Łodziana and M. J. van Setten, *Phys. Rev. B: Condens. Matter*, 2010, **81**, 024117.
40 Y. S. Zhang, E. Majzoub, V. Ozolins and C. Wolverton, *J. Phys. Chem. C*, 2012, **116**, 10522–10528.
41 Y. Nakamori, H. W. Li, K. Kikuchi, M. Aoki, K. Miwa, S. Towata and S. Orimo, *J. Alloys Compd.*, 2007, **446**, 296–300.
42 Y. Nakamori, K. Miwa, A. Ninomiya, H. W. Li, N. Ohba, S. I. Towata, A. Zuttel and S. I. Orimo, *Phys. Rev. B: Condens. Matter*, 2006, **74**, 045126.
43 K. Miwa, N. Ohba, S.-i. Towata, Y. Nakamori and S.-i. Orimo, *Phys. Rev. B: Condens. Matter*, 2006, **69**, 245120.
44 Y. Nakamori, H. Li, M. Matsuo, K. Miwa, S. Towata and S. Orimo, *J. Phys. Chem. Solids*, 2008, **69**, 2292–2296.
45 O. Holloczki, F. Malberg, T. Welton and B. Kirchner, *Phys. Chem. Chem. Phys.*, 2014, **16**, 16880–16890.
46 R. H. Crabtree, *Energy Environ. Sci.*, 2008, **1**, 134–138.
47 D. Teichmann, W. Arlt, P. Wasserscheid and R. Freymann, *Energy Environ. Sci.*, 2011, **4**, 2767–2773.